Electronic Supplementary Material (ESI) for Soft Matter.

Programming Interactions in Magnetic Handshake Materials – Supplement Information

Chrisy Xiyu Du,[1] Hanyu Alice Zhang,[2] Tanner Pearson,[3] Jakin Ng,[3] Paul McEuen,[3,4] Itai Cohen,[3,4] and Michael P. Brenner[1]

[1]*School of Engineering and Applied Sciences, Harvard University, Cambridge, MA, 02139, USA*

[2]*School of Applied and Engineering Physics, Cornell University, Ithaca, NY, 14853, USA*

[3]*Department of Physics, Cornell University, Ithaca, NY, 14853, USA*

[4]*Laboratory of Atomic and Solid-State Physics, Cornell University, Ithaca, NY, 14853, USA*

(Dated: August 5, 2022)

S1. INFORMATION CAPACITY MEASUREMENT

Following the derivation in the Supplementary Information (SI) from [1], we lay out here the steps of obtaining the analytical expression for the effective number (M_{eff}) of non-crosstalk lock-key pairs as a function of number (M) of lock-key pairs and the difference (Δ) of on target and off-target binding energy distribution.

Using the definition in the main text, where we have a set of lock ($x_1, x_2, \ldots, x_M \in X$) and key ($y_1, y_2, \ldots, y_M \in Y$) pairs, with the binding energy matrix $E_{ij} \equiv E(x_i, y_j)$. Similarly, we define the distribution of the energy gap Δ as $\Delta = E_{ij} - s_{ii}$, where E_{ij} is the off-target binding energy between lock i and key j, while s_{ii} is the on-target binding energy between lock i and key i. Note that, in our construction here, s_{ii} does not need to equal to s_{jj}, as a result of the long-range nature of dipole-dipole interaction. However, the distribution of s is very narrow in the range of parameters of interest, so for the simplicity in the derivation, we denote $\bar{s} = \langle s \rangle$ to use in the following derivation.

In this derivation, we assume equal concentration of all lock and key pairs, so the binding probability between lock i and key j can be written as $p(x_i, y_j) = e^{-\beta E_{ij}}/Z$, where β is the inverse temperature, and the partition function Z is expressed as

$$\begin{aligned} Z &= \sum_{x_i \in X, y_j \in Y} e^{-\beta E_{ij}} \\ &= \sum_{x_i} \left(e^{-\beta s_{ii}} + \sum_{y_j, j \neq i} e^{-\beta(\Delta_{ij} + s_{ii})} \right) \\ &= \sum_{x_i} e^{-\beta s_{ii}} \left(1 + \sum_{j \neq i} e^{-\beta \Delta_{ij}} \right) \\ &= e^{-\beta \bar{s}} \sum_{x_i} \left(1 + \sum_{j \neq i} e^{-\beta \Delta_{ij}} \right). \end{aligned} \tag{S1}$$

When we draw M lock and key pairs randomly from the ensemble, we can compute the total probability $p(x_i)$ of finding x_i in a bound pair (marginal distribution of x_i) by taking the average of Z:

$$\langle Z \rangle = e^{-\beta \bar{s}} M [1 + (M-1) \langle e^{-\beta \Delta} \rangle] \tag{S2}$$

Using Eq. S2, we can compute $p(x_i)$ to be

$$\begin{aligned} p(x_i) &= \frac{e^{-\beta s_{ii}}}{Z}\left(1+\sum_{j\neq i} e^{-\beta\Delta_{ij}}\right) \\ &\approx \frac{e^{-\beta\bar{s}}}{\langle Z\rangle}[1+(M-1)\langle e^{-\beta\Delta}\rangle] \\ &= \frac{1}{M}. \end{aligned} \tag{S3}$$

Similarly, we have $p(y_j)\approx 1/M$.

Now we can write the mutual information of the mixture of M lock and key pairs as a function of M and the Δ distribution:

$$\begin{aligned} I(M) &= \sum_{x_i\in X, y_j\in Y} p(x_i,y_j)\log\frac{p(x_i,y_j)}{p(x_i)p(y_j)} \\ &= \sum_{x_i}\left[p(x_i,y_i)\log\frac{p(x_i,y_i)}{p(x_i)p(y_i)} + \sum_{y_j,j\neq i} p(x_i,y_j)\log\frac{p(x_i,y_j)}{p(x_i)p(y_j)}\right] \\ &= \sum_{x_i}\left[\frac{e^{-\beta\bar{s}}}{\langle Z\rangle}\log\frac{e^{-\beta\bar{s}}/\langle Z\rangle}{(1/M)^2} + \sum_{y_j,j\neq i}\frac{e^{-\beta(\Delta_{ij}+\bar{s})}}{\langle Z\rangle}\log\frac{e^{-\beta(\Delta_{ij}+\bar{s})}/\langle Z\rangle}{(1/M)^2}\right] \\ &= \sum_{x_i}\left[\frac{1}{M[1+(M-1)\langle e^{-\beta\Delta}\rangle]}\log\frac{M}{1+(M-1)\langle e^{-\beta\Delta}\rangle} + \right. \\ &\qquad \left. \sum_{y_j,j\neq i}\frac{e^{-\beta\Delta_{ij}}}{M[1+(M-1)\langle e^{-\beta\Delta}\rangle]}\log\frac{Me^{-\beta\Delta_{ij}}}{1+(M-1)\langle e^{-\beta\Delta}\rangle}\right] \end{aligned} \tag{S4}$$

Taking the expected value of the sums in Eq. S4, we can simplify the expression of $I(M)$ to be

$$\begin{aligned} I(M) &= \frac{1}{1+(M-1)\langle e^{-\beta\Delta}\rangle}\log\frac{M}{1+(M-1)\langle e^{-\beta\Delta}\rangle} \\ &\quad + \frac{(M-1)\langle e^{-\beta\Delta}\rangle}{1+(M-1)\langle e^{-\beta\Delta}\rangle}\log\frac{M}{1+(M-1)\langle e^{-\beta\Delta}\rangle} - \frac{(M-1)\langle\beta\Delta e^{-\beta\Delta}\rangle}{1+(M-1)\langle e^{-\beta\Delta}\rangle} \\ &= \log\frac{M}{1+(M-1)\langle e^{-\beta\Delta}\rangle} - \frac{(M-1)\langle\beta\Delta e^{-\beta\Delta}\rangle}{1+(M-1)\langle e^{-\beta\Delta}\rangle} \qquad \text{(S5)} \\ &= \log M_{\text{eff}}. \qquad \text{(S6)} \end{aligned}$$

Combining Eq. S5 and Eq. S6, we get

$$M_{\text{eff}}(M) = \frac{M}{1+(M-1)\langle e^{-\beta\Delta}\rangle}e^{-\frac{(M-1)\langle\beta\Delta e^{-\beta\Delta}\rangle}{1+(M-1)\langle e^{-\beta\Delta}\rangle}}. \tag{S7}$$

In this expression, we are not making any assumptions about how many distinct patterns we could have for a given lock-key system, but rather answering the question that, assuming we can draw as many lock-key as possible that obeys the Δ distribution, how many non-crosstalk pairs can there be.

If we make the assumption that there is enough specificity ($\langle\Delta\rangle > 1k_{\mathrm{B}}T$)in our lock-key system, we can solve for the number (M_c) of lock-key pairs we need to achieve maximum effective lock-key pairs in Eq. S7, which has the form:

$$M_c = \frac{(1+\langle e^{-\beta\Delta}\rangle)^2}{\langle\beta\Delta e^{-\beta\Delta}\rangle - \langle e^{-\beta\Delta}\rangle + \langle e^{-\beta\Delta}\rangle^2} \tag{S8}$$

Using Eq. S7 and Eq. S8, we can predict for the upper bound of how many lock-key pairs we could have for an N-dipole system.

From Eq. S8, we see that M_c depends on the magnitude of Δ, taking the limit of $\langle\Delta\rangle \equiv \mu \to \infty$, we get

$$\begin{aligned} M_c &\approx \frac{1+2e^{-\beta\mu}+e^{-2\beta\mu}}{\beta\mu e^{-\beta\mu} - e^{-\beta\mu} + e^{-2\beta\mu}} \\ &= \frac{e^{2\beta\mu}(1+2e^{-\beta\mu}+e^{-2\beta\mu})}{\beta\mu e^{\beta\mu} - e^{\beta\mu} + 1} \\ &\sim \frac{e^{\beta\mu}}{\beta\mu} \end{aligned} \tag{S9}$$

Eq. S9 tells us that M_c roughly scales exponentially with binding energy, which means that as we increase binding energy, either by printing stronger dipoles or more dipoles, we can increase M_c. However, too strong of a bond might break the equilibrium assumption of our self-assembly process. In the following session, we show the relationship between M_c and magnetic strands and panels of different strengths.

S2. BINDING ENERGY BETWEEN TWO PANELS

We can write down the generalized binding energy expression for both the 1D Magnetic Strand and 2D Magnetic Panel, provided that the nearest neighbor distance within a single strand/panel is fixed to be a. The binding energy follows the form:

$$V = -\frac{\mu_0 m^2}{2\pi d^3}\left[N + k\cdot\frac{d^3}{a^3}\cdot\frac{2d^2/a^2-1}{(1+d^2/a^2)^{5/2}} + \mathcal{F}_3\left(\frac{d}{a}+\right) + \mathcal{F}_4\left(\frac{d}{a}\right) + \cdots\right] \tag{S10}$$

Here μ is vacuum permeability, m is the magnitude of the magnetic dipole moments, d is the separation between two interacting strands/panels, N is the number of dipoles on a single

strand/panel, k is the number of second-nearest neighbor aligned dipole pairs subtract the anti-aligned dipole pairs, $\mathcal{F}_3$ is the effect of third neighbor interactions, and $\mathcal{F}_4 + \cdots$ are the effects of fourth and higher neighbor interactions. We arrived at the final form of Eq. S10 by adding each neighboring effects.

1. Nearest Neighbor Contribution

For nearest neighbor contributions, we only have dipoles that are point in the same direction with separation d. For panel with N dipoles, the contribution can be written as

$$\mathcal{F}_1 = -\frac{\mu_0 m^2 N}{2\pi d^3} \tag{S11}$$

From the equation, we can see that this contribution does not depend on a.

2. Second Nearest Neighbor Contribution

Assume that all dipoles have at least one neighbor at distance a, the separation between the two dipoles can be written as $|\vec{r_{ij}}| = (a^2 + d^2)^{1/2}$. Since for second nearest neighbor, the dipoles do not have to point in the same direction, there are two cases for 2nd nearest neighbor contribution.

Case 1: two dipoles point the same direction.

$$\begin{aligned}
\mathcal{F}_2 &= -\frac{\mu_0}{4\pi|\vec{r_{ij}}|^3}\left[\frac{3d^2m^2}{|\vec{r_{ij}}|^2} - m^2\right] \\
&= -\frac{\mu_0 m^2}{4\pi|\vec{r_{ij}}|^5}\left[3d^2 - (a^2+d^2)\right] \\
&= -\frac{\mu_0 m^2}{4\pi}\left[\frac{2d^2 - a^2}{(a^2+d^2)^{5/2}}\right]
\end{aligned} \tag{S12}$$

Case 2: two dipoles point different directions.

$$\begin{aligned}
\mathcal{F}_2 &= -\frac{\mu_0}{4\pi|\vec{r_{ij}}|^3}\left[\frac{-3d^2m^2}{|\vec{r_{ij}}|^2} + m^2\right] \\
&= -\frac{\mu_0 m^2}{4\pi|\vec{r_{ij}}|^5}\left[(a^2+d^2) - 3d^2\right] \\
&= -\frac{\mu_0 m^2}{4\pi}\left[\frac{a^2 - 2d^2}{(a^2+d^2)^{5/2}}\right]
\end{aligned} \tag{S13}$$

From the previous two expressions, we can see that the second nearest neighbor distance is always in the form of $(a^2 + d^2)^{1/2}$, and it does not depend on the underline lattice that

the dipoles are on. The only assumption we made here is that every dipole has at least one nearest neighbor at distance a within the panel.

Also, if we look at the contribution from case 1 and 2, we see that they completely cancel each other out. So depending on how many pairs of case 1 and case 2 second nearest neighbors we have, we might get different integer pre-factors for this contribution, or this term can be completely canceled out if we have the same number of case 1 and 2 pairs.

Lastly, we see that, at $d = \sqrt{2}a/2$, the contribution from second nearest neighbors completely cancel out despite how many pairs of case 1 and 2.

3. Third Nearest Neighbor Contribution

Third nearest neighbor contributions will depend on the underline lattice of the dipoles. Here, we will discuss two scenarios: square and triangular lattice.

For **square lattice**, the 3rd nearest neighbor $|\vec{r_{ij}}| = (2a^2 + d^2)^{1/2}$. Following the same derivation, we can write the two case contributions as:

Case 1: two dipoles point the same direction.

$$\mathcal{F}_3 = -\frac{\mu_0 m^2}{4\pi}\left[\frac{2d^2 - 2a^2}{(2a^2 + d^2)^{5/2}}\right] \tag{S14}$$

Case 2: two dipoles point opposite directions.

$$\mathcal{F}_3 = -\frac{\mu_0 m^2}{4\pi}\left[\frac{2a^2 - 2d^2}{(2a^2 + d^2)^{5/2}}\right] \tag{S15}$$

For **triangular lattice**, the 3rd nearest neighbor $|\vec{r_{ij}}| = (3a^2 + d^2)^{1/2}$. Following the same derivation, we can write the two case contributions as:

Case 1: two dipoles point the same direction.

$$\mathcal{F}_3 = -\frac{\mu_0 m^2}{4\pi}\left[\frac{2d^2 - 3a^2}{(3a^2 + d^2)^{5/2}}\right] \tag{S16}$$

Case 2: two dipoles point opposite directions.

$$\mathcal{F}_3 = -\frac{\mu_0 m^2}{4\pi}\left[\frac{3a^2 - 2d^2}{(3a^2 + d^2)^{5/2}}\right] \tag{S17}$$

Since in our final design, we do not confine the dipole patterns on a given geometry, there is no universal form of the third and higher neighbor interactions. We thus indicate them as a function of d/a.

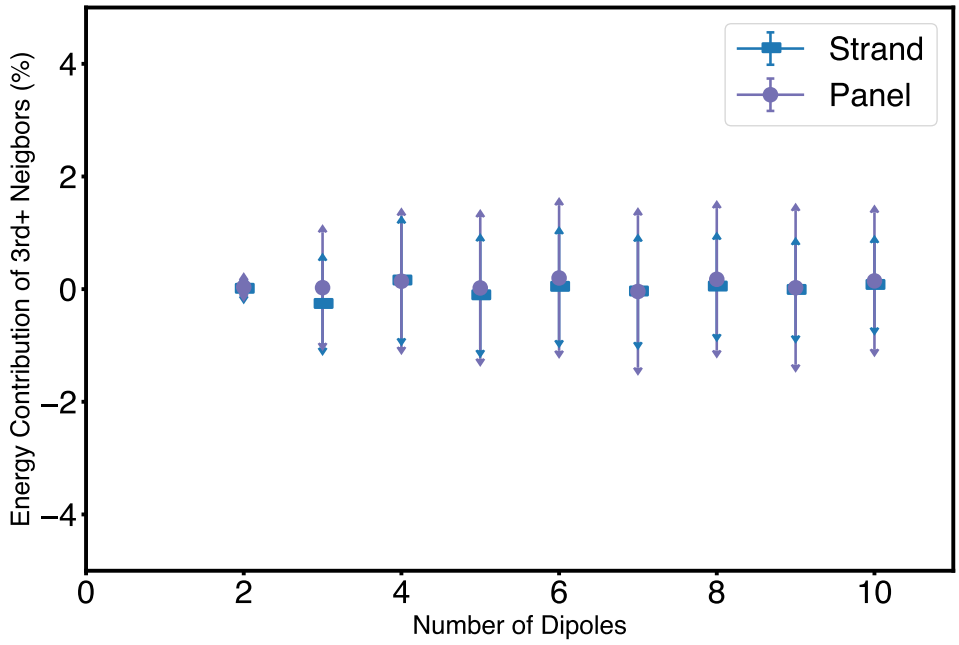

FIG. S1. Energy contribution from third and higher neighbor interactions for strands and panels with $N = 2 - 10$ dipoles.

In addition, for dipole pattern designs ($d/a = \sqrt{2}/2$) within this study, the major contribution of the energy comes from nearest-neighbor alone as all second-nearest neighbor interaction cancels out by the argument presented above, and third and higher neighbor interactions contribute around 2% of the total binding energy (see Fig. S1).

S3. SHAPE OF Δ DISTRIBUTION

Eq. S10 gives us two parameters we could play with while investigating the information capacity of our magnetic systems. The first one being $\frac{\mu_0 m^2}{2\pi d^3}$, which dictates the energy level of our system, and the second one being d/a, which dictates the shape of the Δ distribution. Fig. S2 shows the shape of the Δ distribution of magnetic strands and panels with $N = 2-10$ dipoles.

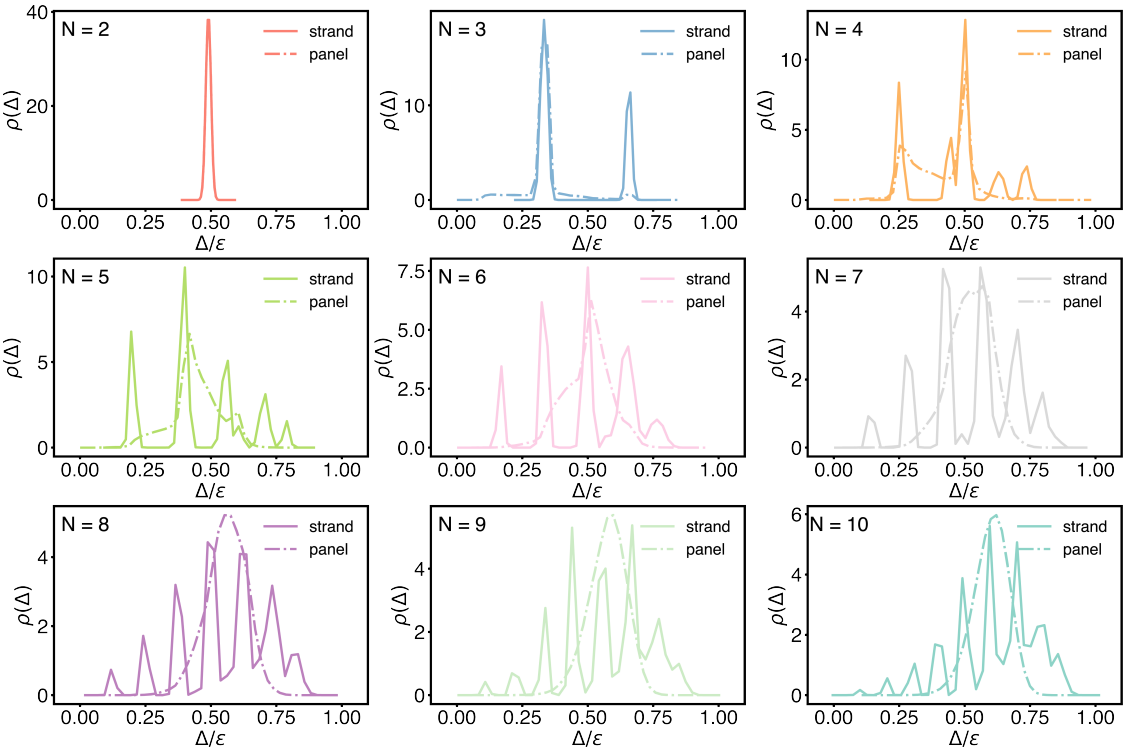

FIG. S2. Δ distribution comparison in the unit of total binding energy ϵ for 1D Magnetic Strand and 2D Magnetic Panel varying N from 2 to 10.

A. Δ for 1D Magnetic Strand

Fig. S3(a) shows the cumulative Δ distribution for 1D Magnetic Strands. Here the distribution is exact, as we obtained the binding energy matrix for all distinct strands for systems with $N = 2 - 10$ dipoles. We can see that the distribution is not smooth, but rather has steps with step size roughly correlates to $1/N$, which is an indication of the underlying geometry of the 1D strand.

B. Δ for 2D Magnetic Panel

Fig. S3(b) shows the cumulative Δ distribution for 2D Magnetic Panels. The distribution here is not exact, but an estimation of the binding energy profile based on 1500 randomly generated panels with $N = 2 - 10$ dipoles. We can see that curve shifts right as we increase the number of dipoles in our panel, which tells us that no only the whole system gets a higher binding energy as we put more dipoles on a panel, we also decrease crosstalk per

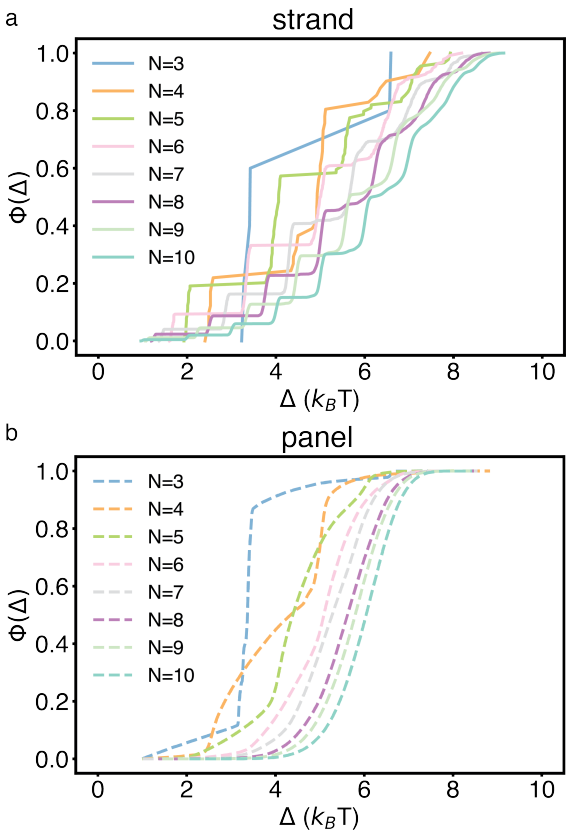

FIG. S3. (a) Cumulative Δ distribution for 1D Magnetic Strand. Here everything is plotted with a total binding energy $\epsilon = 10k_{\mathrm{B}}T$. (b) Cumulative Δ distribution for 2D Magnetic Panel. Here everything is plotted with a total binding energy $\epsilon = 10k_{\mathrm{B}}T$.

dipole.

In addition, we can take a closer look at how the Δ distribution changes as we move from 1D strand to 2D panel. Fig. S2 shows the Δ distribution of the same number of dipoles between strand and panel. We note that when $N = 2$, the distribution is identical, which is consistent as for $N = 2$, panel and strand systems are completely identical. As we increase N, Δ becomes much smoother as we open up more possibilities of arranging dipoles on a 2D surface.

S4. LARGE N LIMIT

Since we are fixing the total binding energy to be $10k_{\mathrm{B}}T$, the information capacity of the system solely depends on the shape of the Δ distribution assuming there are much more

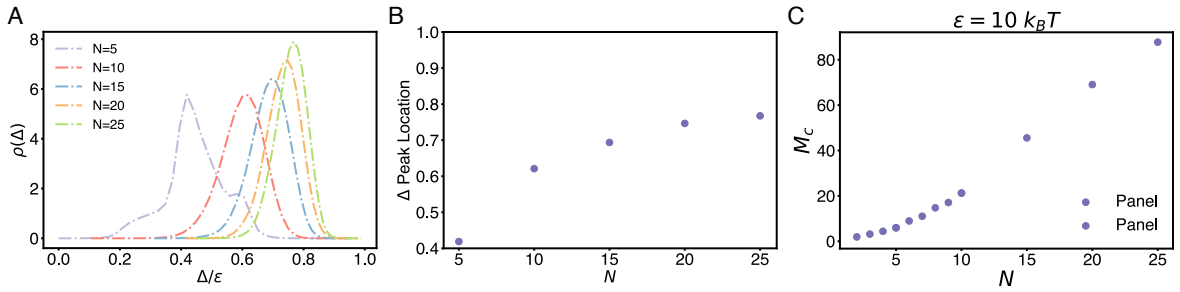

FIG. S4. A. Δ distribution for panel systems with $N = [5, 10, 15, 20, 25]$ dipoles. B. Δ peak locations for panel systems with $N = [5, 10, 15, 20, 25]$ dipoles, C. M_c for panel systems with $N = [2 - 10, 15, 20, 25]$ dipoles at $\epsilon = 10k_{\mathrm{B}}T$.

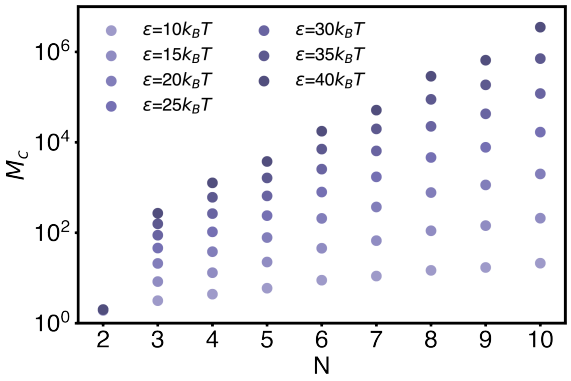

FIG. S5. The dependence of M_c as a function of number (N) of dipoles on panel for different total binding energy ϵ.

different lock-key patterns compare to the effective non-crosstalk (M_c) patterns. In Fig. S4A, we plot the Δ distribution for panel systems with $N = [5, 10, 15, 20, 25]$ dipoles. We notice that, the location of the Δ distribution peak keep shifting towards 1 (1 means there is no crosstalk) as we increase the number of dipoles (Fig. S4B), but the shift gets smaller and smaller. Simiarly, in Fig. S4C, we notice a slow down in the M_c increase as a function of N.

Because we are fixing the total binding energy, after some large N, increasing N will not dramatically shift the peak of the Δ distribution any more and that's where we will hit the limit of effective number of non-crosstalk interactions. The exact value of this large N is very system dependent and could be interesting for future study.

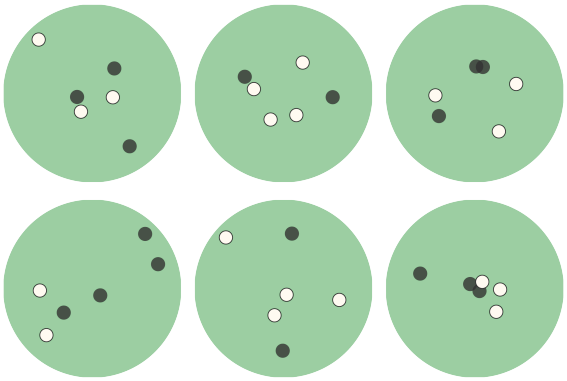

FIG. S6. Sample randomly generated dipole patterns with $N = 6$ dipoles.

S5. M_c DEPENDENCY OF BINDING ENERGY

Fig. S5 shows M_c for different binding energies. We see that as we increase binding energy, M_c increases faster as a function of N.

S6. MAGNETIC PANEL GENERATION

We used two different methods to generate dipole patterns for 2D panels: complete random generation and fixed d/a ration generation. The complete random generation method is used as a benchmark to demonstrate that fixed d/a ratio method yields higher M_c.

A. Complete Random Generation

For complete random generation, we randomly place N dipoles within a square of area N, so that the density of dipoles remains the same for panels with different number of dipoles. After obtaining the positions of the dipoles, we randomly assign a direction for each dipole. Fig. S6 shows a few examples of randomly generated dipole patterns with 6 dipoles.

B. Fixing d/a Ratio

For dipole patterns with fixed d/a ratio, we generate dipole patterns with N dipoles with the following steps:

1. Put down the first dipole at position $[0, 0, 0]$

2. Before we have N dipoles, we randomly choose one of the existing dipoles

3. We put down a new dipole at distance a away from the chosen dipole

4. We make sure that this new dipole is at least distance a away from all other dipoles

5. Repeat the process till we have N dipoles

S7. SIMULATION MODEL

We perform dimer assembly to validate our panel designs and perform a finite square simulation to showcase the possibility in using our magnetic panels for heterogeneous assembly. For our simulation model, we coarse grain the dipole patterns into an attractive interaction patch [2] with strength based on the binding energy matrix with a WCA potential to mimic steric interactions. The attractive interaction patch has an opening angle of 60 degrees to ensure single bond formation.

For both the dimer (Fig. S7) and square assembly, we used the standard NVT integrator with a randomized velocity at initialization. We slowly compress the simulation box to the targeted area fraction at a high temperature to guarantee a random initial state, then we slowly equilibrate the system for 10^6 steps to the targeted temperature. Finally, for dimer assembly, we run 5×10^6 steps for the system to fully equilibrate and 2×10^7 steps for the finite square assembly.

All simulations are performed using HOOMD-blue [3–5], while we used Freud [6] for data analysis, and Signac [7, 8] for data management.

A. Dipole Patterns for 10-Dipole System

Fig. S8 shows the dipole patterns we used to compute the binding energy matrix for the 3×3 square assembly.

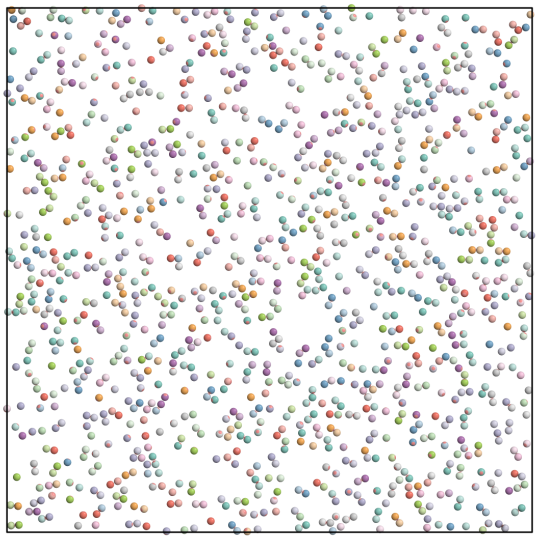

FIG. S7. Snapshot for dimer self-assembly.

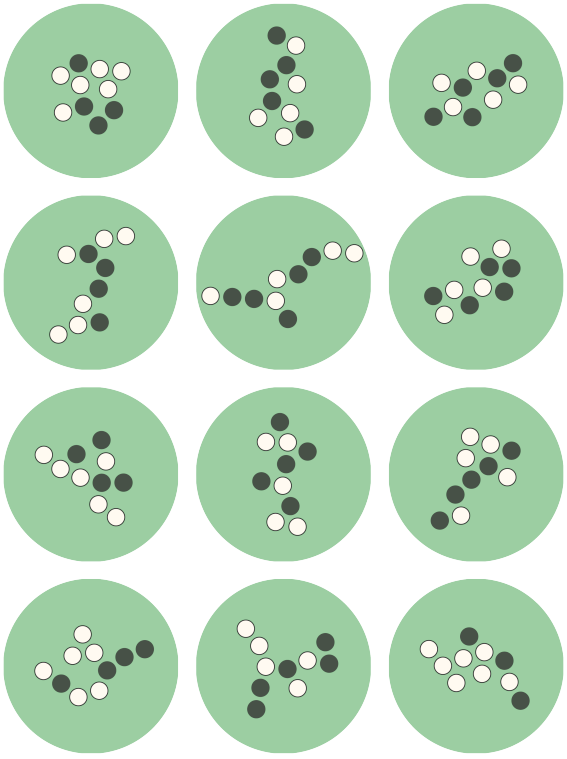

FIG. S8. 10-Dipole patterns used for 3×3 panel assembly.

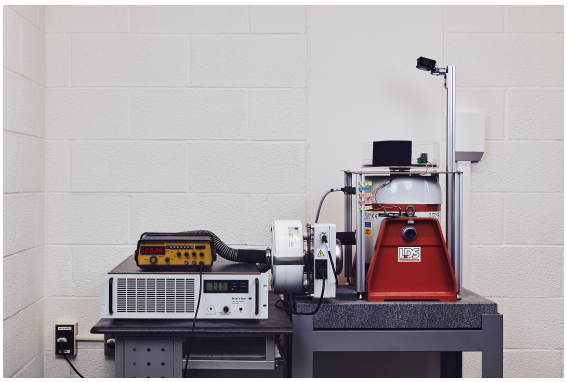

FIG. S9. Photo of experimental setup

S8. EXPERIMENTAL SETUP

A. Shaker Setup

The shaker used to perform this experiment is the Brüel & Kjær Linear Power Amplifier LDS LPA 1000. This amplifier takes in a signal from a BK Precision 3011B function generator and amplifies the signal to feed into a Bruel & Kjaer LDS V456 Permanent Magnet Shaker. A bowl with a diameter of 25.4cm (10 in) attached on top of the shaker and used as the arena for experiments. A metal plate is placed in between the shaker and the shaker bowl to provide magnetic shielding. During the experiments, a GoPro Hero 5 is mounted above the shaker bowl to take videos. A photo of this setup is shown in Figure S9.

B. Calibration

The frequency we used for these experiments was 25 Hz. For all experiments, the frequency was set to this value and the amplitude of the sine wave is varied with function generator for fine control or the amplifier for coarse control. All systems had finalized a and d values of $a = 2.8$mm (0.11 inches) and $d = 2$mm (0.079 inches), giving a d/a ratio between 0.71 and 0.72.

To keep these experiments 2-dimensional, a top plate of laser-cut acrylic was added onto the setup. The height of the top plate needs to be such that there is enough room under the plate to allow for the systems to bounce around, but the plate needs to be low enough to keep the experiments roughly 2-dimensional. To account for the different shapes and

dimensions of the dimers versus the square assembly panels, the height of the plate was set to different values for these two experiments.

The acceleration of the shaker is measured by an Adafruit Triple-Axis Accelerometer ADXL345 with an empty shaker bowl. The shaker was left at a shaker setting for 5 minutes and an Arduino Uno board was used to sample the accelerometer every 15 milliseconds. This data is monitored with a laptop through the Serial Monitor and copied into a text editor. Python code is then used to parse the `.txt` document and calculate the rms values reported in this paper.

C. Boundary Condition

For all the experiments, all the panels are being confined in a fixed area by an acrylic cylindrical boundary to ensure a $\sim 20\%$ area density, so there are no magnetically responding materials at the system boundary or beyond. The magnets used in the experiments are permanent neodymium-iron-boron grade and the magnetic moment is fixed by gluing the magnets into holes in the rigid panel. Care was taken to magnetically shield the panels from the magnetic field produced by the shaker coil. As such, there is no external magnetic field applied. Moreover, the field produced by the other panels is extremely weak because panels are well separated and randomly oriented with some dipoles pointing in opposite directions even within the same panel. As such there is no magnetic field in the experiment that is sufficient to demagnetize the magnets within our panels over the time scale of our experiments, which is roughly 30min.

D. Lock and Key Manufacture Process

The magnets used are N40 cylindrical magnets with diameter 1.6 mm (1/16 in) and height 0.8 mm (1/32 in) from magcraft, serial number NSN0591. Holes with diameter 1.6 mm (0.062 in) and nearest neighbor center to center distances of 2.8 mm (0.11 in) are engraved onto the acrylic sheets and the magnets are press-fitted into the holes in accordance with the designed dipole patterns. After the magnets are pressed in, 8 sheets of 0.08 mm (0.003 in, 3 mil) thick laminate was stuck on top of the magnets to achieve the desired d/a value.

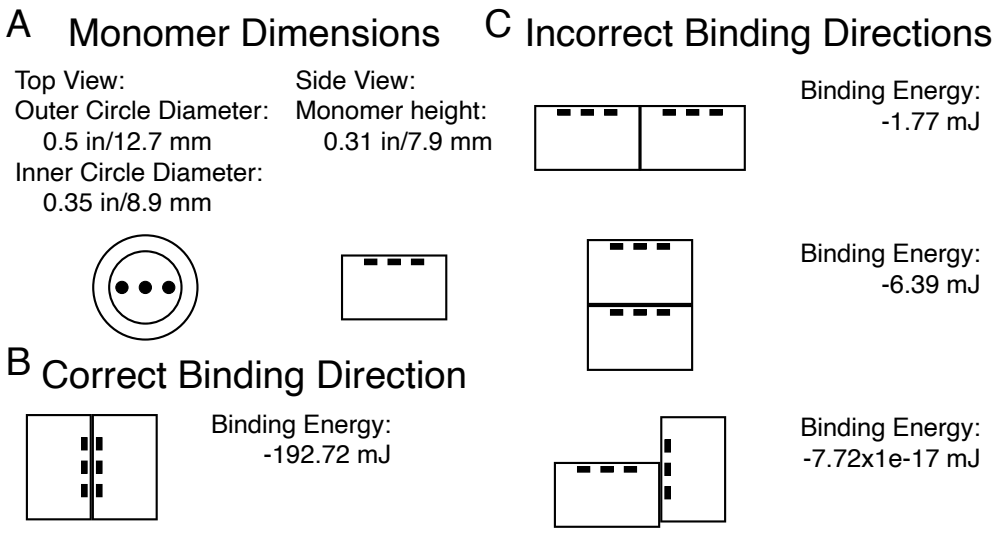

FIG. S10. A. Final monomer dimensions for dimer self-assembly. B. Correct dimer binding configuration and its binding energy. C. Top three Incorrect binding configurations and their binding energy.

E. Dimer Self-Assembly

The final dimer dimensions we decided on were circular disks with diameter 12.7 mm (0.5 in). They were laser cut from acrylic and glued on top of each other to form a dimer panel with a height of 7.9 mm (0.31 in). Holes for the magnets were centered in the circular disks and cut in accordance with the dimensions above.

We decided on this final dimer dimensions to reduce all possible incorrect binding configurations between the targeted lock-key pairs. Fig. S10A shows the dimensions for the monomers and their dipole placements. Fig. S10B shows the correct binding configuration while Fig. S10C shows the top three incorrect binding configurations. We note that the correct binding energy is at least 30 times more than any of the incorrect binding energies, proving our design is efficient enough to prevent undesired binding configurations.

To run the experiments, a top plate was mounted with spacers 16.8 mm (0.66 in) above the shaker base, and the systems were allowed to vibrate freely within the enclosure. The spacers have a width of 7.6 mm (0.3 in), which brings the usable diameter in the shaker during the experiments down to 23.9 cm (9.4 in). By using 4 sets of the 12 designed 3-dipole lock and key pairs, we obtain a fill fraction of $\frac{1.27\times0.79\times12\times2\times4}{\pi\times(23.9/2)^2} = 21\%$.

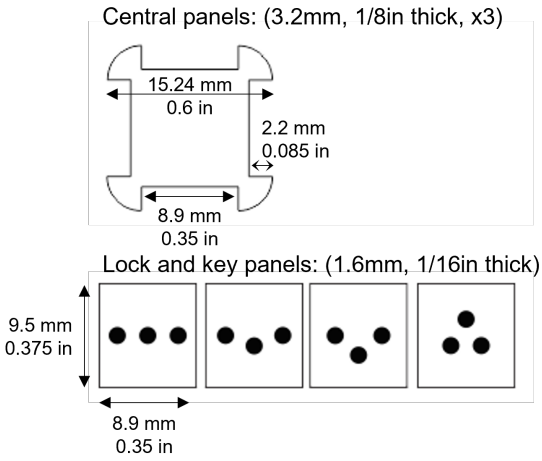

FIG. S11. CorelDraw patterns for laser cutting the square panel self assembly system.

F. Finite Square Self-Assembly

For the finite square self-assembly experiment, we cut out lock and key panels to hold the magnets and also central panels to attach the lock and key panels to. The lock and key panels are 8.9 mm by 9.5 mm (0.35 in by 0.375 in) rectangular panels with holes for the 12 lock and key combinations, and was cut from 1.6 mm (1/16 in) thick acrylic. For the central panels, we used squares with rounded corners and a side length of 15.24 mm (0.6 in) with slots 2.2 mm (0.085 in) deep on the sides, where the lock and key panels were glued. The central panels are cut from 3.2 mm (1/8 in) thick acrylic and three were glued on top of each other to form final panels with height 9.5 mm (0.38 in). Figure S11 shows the laser cut files with dimensions.

This experiment utilized a top plate mounted 16 mm (0.63 in) above the shaker base. In order to run experiments in parallel, 4 sets of panels were made, and 4 arenas with inner diameters of 88.9 mm (3.5 in) were cut and taped into the shaker bowl. With these dimensions, we can calculate a fill fraction of $\frac{16^2 \times 9}{\pi \times (88.9/2)^2} = 37\%$ for each experiment.

G. Data Collection

To decide on the final shaker amplitudes to use for the experiments, we put the systems in the shaker and tuned the amplitude to find a value where the correct bonds are just able to form and stick together. This allowed us to obtain an optimal shaker amplitude of around

0.7A (acceleration rms 2.4g) for both the dimer and square panel experiments. After the optimal value of 0.7A was found, we decided to collect data for shaker settings in increments of 0.1A for the dimers, and 5 sets of data was collected for shaker settings of 0.4, 0.5, 0.6, 0.7, 0.8, 0.9, 1.0, and 1.1A each. For the square panel assembly, we found that the optimal setting was at a sweet spot right on the transition between 0.6A and 0.7A, so the shaker was set at 0.7A but close to the transition to 0.6A. Under this protocol, 25 experiments were run, giving us 100 sets of data.

We ran the experiments by bringing the systems to an amplitude where no bonds can form, and then setting the shaker amplitude to the desired value for the experiment. After running each experiment for 30 minutes, the system was quenched and the bonds are then manually counted and reported in the main text.

---

[1] M. H. Huntley, A. Murugan, and M. P. Brenner, Information capacity of specific interactions, Proceedings of the National Academy of Sciences **113**, 5841 (2016).

[2] D. J. Beltran-Villegas, B. A. Schultz, N. H. Nguyen, S. C. Glotzer, and R. G. Larson, Phase behavior of janus colloids determined by sedimentation equilibrium, Soft Matter **10**, 4593 (2014).

[3] J. A. Anderson, J. Glaser, and S. C. Glotzer, Hoomd-blue: A python package for high-performance molecular dynamics and hard particle monte carlo simulations, Computational Materials Science **173**, 109363 (2020).

[4] T. D. Nguyen, C. L. Phillips, J. A. Anderson, and S. C. Glotzer, Rigid body constraints realized in massively-parallel molecular dynamics on graphics processing units, Computer Physics Communications **182**, 2307 (2011).

[5] J. Glaser, X. Zha, J. A. Anderson, S. C. Glotzer, and A. Travesset, Pressure in rigid body molecular dynamics, Computational Materials Science **173**, 109430 (2020).

[6] V. Ramasubramani, B. D. Dice, E. S. Harper, M. P. Spellings, J. A. Anderson, and S. C. Glotzer, freud: A software suite for high throughput analysis of particle simulation data, Computer Physics Communications **254**, 107275 (2020).

[7] C. S. Adorf, P. M. Dodd, V. Ramasubramani, and S. C. Glotzer, Simple data and workflow management with the signac framework, Comput. Mater. Sci. **146**, 220 (2018).

[8] V. Ramasubramani, C. S. Adorf, P. M. Dodd, B. D. Dice, and S. C. Glotzer, signac: A Python

framework for data and workflow management, in *Proceedings of the 17th Python in Science Conference* (2018) pp. 152–159.